JOURNAL OF OPTIMIZATION THEORY AND APPLICATIONS: Vol. 95, No. 3, pp. 467-499, DECEMBER 1997

Optimal Trajectories for Earth-to-Mars Flight[1]

A. MIELE[2] AND T. WANG[3]

Abstract. This paper deals with the optimal transfer of a spacecraft from a low Earth orbit (LEO) to a low Mars orbit (LMO). The transfer problem is formulated via a restricted four-body model in that the spacecraft is considered subject to the gravitational fields of Earth, Mars, and Sun along the entire trajectory. This is done to achieve increased accuracy with respect to the method of patched conics.

The optimal transfer problem is solved via the sequential gradient-restoration algorithm employed in conjunction with a variable-stepsize integration technique to overcome numerical difficulties due to large changes in the gravitational field near Earth and near Mars. The optimization criterion is the total characteristic velocity, namely, the sum of the velocity impulses at LEO and LMO. The major parameters are four: velocity impulse at launch, spacecraft vs. Earth phase angle at launch, planetary Mars/Earth phase angle difference at launch, and transfer time. These parameters must be determined so that ΔV is minimized subject to tangential departure from circular velocity at LEO and tangential arrival to circular velocity at LMO.

For given LEO and LMO radii, a departure window can be generated by changing the planetary Mars/Earth phase angle difference at launch, hence changing the departure date, and then reoptimizing the transfer. This results in a one-parameter family of suboptimal transfers, characterized by large variations of the spacecraft vs. Earth phase angle at launch, but relatively small variations in transfer time and total characteristic velocity.

For given LEO radius, an arrival window can be generated by changing the LMO radius and then recomputing the optimal transfer. This leads to a one-parameter family of optimal transfers, characterized by small variations of launch conditions, transfer time, and total characteristic velocity, a result which has important guidance implications. Among the members of the above one-parameter family, there is an optimum–optimorum trajectory with the smallest characteristic velocity.

[1]This paper is dedicated to the memory of Professor Placido Cicala of the Polytechnic of Turin, Turin, Italy.

[2]A. J. Foyt Professor Emeritus of Engineering, Aerospace Sciences, and Mathematical Sciences, Rice University, Houston, Texas.

[3]Senior Research Scientist, Aero-Astronautics Group, Rice University, Houston, Texas.

0022-3239/97/1200-0467$12.50/0

This occurs when the radius of the Mars orbit is such that the associated period is slightly less than one-half Mars day.

Key Words. Flight mechanics, astrodynamics, celestial mechanics, Earth-to-Mars missions, departure window, arrival window, optimization, sequential gradient-restoration algorithm.

1. Introduction

The Mars mission is attractive and expensive (Refs. 1–4). An important component of a typical Mars mission is the transfer of a spacecraft from a low Earth orbit (LEO) to a low Mars orbit (LMO). The optimization of such transfer is of interest because optimal trajectories set a benchmark for minimum characteristic velocity, hence minimum propellant consumption; also, launch/arrival windows provide basic information for the development of robust guidance (Refs. 5–13).

This paper addresses four problems: baseline optimal trajectory, departure window, arrival window, and optimum–optimorum trajectory.

(P1) Baseline Optimal Trajectory. For given LEO and LMO radii, the optimization criterion is the total characteristic velocity ΔV, the sum of the velocity impulses at LEO and LMO. Major parameters are four: (i) velocity impulse at launch, (ii) spacecraft vs. Earth phase angle at launch, (iii) planetary Mars/Earth phase angle difference at launch, (iv) transfer time. These parameters must be determined so that ΔV is minimized, subject to the following requirements: tangential departure from circular velocity at LEO; tangential arrival to circular velocity at LMO.

(P2) Departure Window. For given LEO and LMO radii, this study involves the computation of a one-parameter family of suboptimal transfers, obtained by changing the planetary Mars/Earth phase angle difference at launch, hence changing the departure date vis-a-vis the optimal value determined under (P1). The objective is to determine how a change in parameter (iii), hence a change in departure date, affects the optimal values of the remaining parameters.

(P3) Arrival Window. For given LEO radius, this study involves the computation of a one-parameter family of optimal transfers, obtained by changing the LMO radius. The objective is to determine how a change in LMO radius affects the optimal values of parameters (i) to (iv). This study has important guidance implications.

(P4) Optimum–Optimorum Trajectory. For given LEO radius, this study involves the computation of the LMO radius yielding the smallest total characteristic velocity. In this study, the LMO radius is regarded as a variable in addition to parameters (i) to (iv).

Problems (P1) to (P4) are treated within the frame of the restricted four-body model: the spacecraft is considered subject to the gravitational fields of Earth, Mars, and Sun along the entire trajectory. This is done in order to achieve increased accuracy with respect to the method of patched conics. An important difficulty in system integration and optimization is that the total gravitational force changes rapidly in near-Earth space and near-Mars space, but slowly in deep interplanetary space. Indeed, orbital periods are of order one hour to one day if Earth gravity or Mars gravity is dominant, but of order one year if Sun gravity is dominant. This difficulty can be overcome by treating Problems (P1) to (P4) with the sequential gradient-restoration algorithm in conjunction with a variable-stepsize integration technique.

The paper is organized as follows. Section 2 deals with the system description. Sections 3 and 4 deal with the initial and final conditions. Section 5 discusses coordinate system transformation. Section 6 deals with the formulation of the optimal LEO-to-LMO transfer and outlines the computational method. Section 7 contains planetary and spacecraft data used in the numerical experiments. Sections 8–11 provide the numerical results for the baseline optimal trajectory, departure window, arrival window, and optimum-optimorum trajectory. Finally, Section 12 contains the conclusions.

2. System Description

We study the transfer of a spacecraft from a low Earth orbit (LEO) to a low Mars orbit (LMO) under the following assumptions:

- (A1) the Sun is fixed in space;
- (A2) Earth and Mars are subject only to Sun gravity;
- (A3) the eccentricity of the Earth and Mars orbits around Sun is neglected, implying circular planetary motions;
- (A4) the inclination of the Mars orbital plane vis-a-vis the Earth orbital plane is neglected, implying planar spacecraft motion;
- (A5) the spacecraft is subject to the gravitational attractions of Earth, Mars, and Sun;
- (A6) the class of two-impulse trajectories, departing with a tangential velocity impulse from circular velocity at LEO and arriving with a tangential velocity impulse to circular velocity at LMO, is considered.

Having adopted the restricted four-body model to achieve increased precision with respect to the method of patched conics, we are simultaneously interested in five motions: the inertial motions of Earth, Mars, and spacecraft

with respect to Sun; the relative motions of the spacecraft with respect to Earth and Mars. To study these motions, we employ three coordinate systems.

(SCS) Sun Coordinate System. This is a fixed system with the origin at the Sun center S. The x-axis is directed along the line SE_0 connecting the Sun center with the Earth initial position. The y-axis is orthogonal to the x-axis. The Sxy system is fixed in space.

(ECS) Earth Coordinate System. This is a moving system with the origin at the instantaneous Earth center E. The x-axis is directed along the line SE connecting the Sun center and the instantaneous Earth center. The y-axis is orthogonal to the x-axis. The Exy system translates and rotates in space as Earth moves around Sun.

(MCS) Mars Coordinate System. This is a moving system with the origin at the instantaneous Mars center M. The x-axis is directed along the line SM connecting the Sun center and the instantaneous Mars center. The y-axis is orthogonal to the x-axis. The Mxy system translates and rotates in space as Mars moves around Sun.

To sum up, SCS is employed to describe the inertial motions of Earth, Mars, and spacecraft with respect to Sun. On the other hand, ECS and MCS are employed to describe the relative motions of the spacecraft with respect to Earth and Mars.

Let E, M, S denote the centers of Earth, Mars, and Sun; let P denote the spacecraft. Let t denote the time, with $0 \leq t \leq \tau$, where τ is the final time. With this understanding, we describe the motions of Earth, Mars, and spacecraft with respect to Sun; we employ the Sun coordinate system and polar coordinates.

2.1. Earth. Subject only to the Sun gravitational attraction, the motion of Earth (subscript E) around Sun is described by the following differential equations for the radial distance r_E, phase angle ϕ_E, inertial velocity V_E, and path inclination γ_E with respect to the local horizon:

$$\text{(SCS)} \quad dr_E/dt = V_E \sin \gamma_E, \tag{1a}$$

$$d\phi_E/dt = (V_E/r_E) \cos \gamma_E, \tag{1b}$$

$$dV_E/dt = -(\mu_S/r_E^2) \sin \gamma_E, \tag{1c}$$

$$d\gamma_E/dt = (V_E/r_E - \mu_S/V_E r_E^2) \cos \gamma_E, \tag{1d}$$

where μ_S is the Sun gravitational constant. Neglecting the orbital eccentricity, we approximate the Earth trajectory with a circle; hence,

$$r_E = r_E(0), \tag{2a}$$

$$\phi_E = t\sqrt{[\mu_S/r_E^3(0)]} + \phi_E(0), \tag{2b}$$

$$V_E = \sqrt{[\mu_S / r_E(0)]}, \tag{2c}$$

$$\gamma_E = \gamma_E(0) = 0. \tag{2d}$$

2.2. Mars. Subject only to the Sun gravitational attraction, the motion of Mars (subscript M) around Sun is described by the following differential equations for the radial distance r_M, phase angle ϕ_M, inertial velocity V_M, and path inclination γ_M with respect to the local horizon:

$$\text{(SCS)} \quad dr_M/dt = V_M \sin \gamma_M, \tag{3a}$$

$$d\phi_M/dt = (V_M/r_M) \cos \gamma_M, \tag{3b}$$

$$dV_M/dt = -(\mu_S/r_M^2) \sin \gamma_M, \tag{3c}$$

$$d\gamma_M/dt = (V_M/r_M - \mu_S/V_M r_M^2) \cos \gamma_M, \tag{3d}$$

where μ_S is the Sun gravitational constant. Neglecting the orbital eccentricity, we approximate the Mars trajectory with a circle; hence,

$$r_M = r_M(0), \tag{4a}$$

$$\phi_M = t\sqrt{[\mu_S / r_M^3(0)]} + \phi_M(0), \tag{4b}$$

$$V_M = \sqrt{[\mu_S / r_M(0)]}, \tag{4c}$$

$$\gamma_M = \gamma_M(0) = 0. \tag{4d}$$

2.3. Spacecraft. Subject to the gravitational attractions of Sun, Earth, and Mars, the motion of the spacecraft (subscript P) around Sun is described by the following differential equations for the radial distance r_P, phase angle ϕ_P, inertial velocity V_P, and path inclination γ_P with respect to the local horizon:

$$\text{(SCS)} \quad dr_P/dt = V_P \sin \gamma_P, \tag{5a}$$

$$d\phi_P/dt = (V_P/r_P) \cos \gamma_P, \tag{5b}$$

$$\begin{aligned} dV_P/dt = &-(\mu_S/r_P^2) \sin \gamma_P \\ &+ (\mu_E/r_{PE}^2) \cos(\psi_{PE} - \gamma_P) \\ &+ (\mu_M/r_{PM}^2) \cos(\psi_{PM} - \gamma_P), \end{aligned} \tag{5c}$$

$$\begin{aligned} d\gamma_P/dt = &(V_P/r_P - \mu_S/V_P r_P^2) \cos \gamma_P \\ &+ (\mu_E/V_P r_{PE}^2) \sin(\psi_{PE} - \gamma_P) \\ &+ (\mu_M/V_P r_{PM}^2) \sin(\psi_{PM} - \gamma_P). \end{aligned} \tag{5d}$$

Here μ_S, μ_E, μ_M are the gravitational constants of Sun, Earth, and Mars; r_{PE} and r_{PM} are the radial distances of the spacecraft from Earth and Mars; ψ_{PE} and ψ_{PM} are the inclinations of the vectors PE and PM (hence, the inclinations of the vectors g_{PE} and g_{PM}) with respect to the local horizon. These quantities are given by the following relations, obtainable via simple geometric considerations:

$$r_{PE}^2 = r_P^2 + r_E^2 - 2r_P r_E \cos(\phi_P - \phi_E), \tag{6a}$$

$$r_{PM}^2 = r_P^2 + r_M^2 - 2r_P r_M \cos(\phi_P - \phi_M), \tag{6b}$$

$$\sin \psi_{PE} = -r_P/r_{PE} + (r_E/r_{PE}) \cos(\phi_P - \phi_E), \tag{6c}$$

$$\cos \psi_{PE} = -(r_E/r_{PE}) \sin(\phi_P - \phi_E), \tag{6d}$$

$$\sin \psi_{PM} = -r_P/r_{PM} + (r_M/r_{PM}) \cos(\phi_P - \phi_M), \tag{6e}$$

$$\cos \psi_{PM} = -(r_M/r_{PM}) \sin(\phi_P - \phi_M), \tag{6f}$$

with the implication that the trigonometric expressions in Eqs. (5c) and (5d) can be rewritten as

$$\sin(\psi_{PE} - \gamma_P) = -(r_P/r_{PE}) \cos \gamma_P + (r_E/r_{PE}) \cos(\phi_P - \phi_E - \gamma_P), \tag{6g}$$

$$\cos(\psi_{PE} - \gamma_P) = -(r_P/r_{PE}) \sin \gamma_P - (r_E/r_{PE}) \sin(\phi_P - \phi_E - \gamma_P), \tag{6h}$$

$$\sin(\psi_{PM} - \gamma_P) = -(r_P/r_{PM}) \cos \gamma_P + (r_M/r_{PM}) \cos(\phi_P - \phi_M - \gamma_P), \tag{6i}$$

$$\cos(\psi_{PM} - \gamma_P) = -(r_P/r_{PM}) \sin \gamma_P - (r_M/r_{PM}) \sin(\phi_P - \phi_M - \gamma_P). \tag{6j}$$

These expressions allow one to avoid the computation of the angles ψ_{PE} and ψ_{PM} in Eqs. (5c) and (5d).

2.4. Remark. In Eqs. (1)–(6), the ϕ-angles are measured starting from the radial direction and are positive counterclockwise. The ψ-angles and γ-angles are measured starting from the local horizon and are positive clockwise.

3. Initial Conditions

Let $t = 0$ denote the initial time. With this understanding, we state the initial conditions for Earth, Mars, and spacecraft.

3.1. Earth. In the Sun coordinate system, the Earth initial conditions ($t=0$) are given by

$$\text{(SCS)} \quad r_E(0) = \text{given}, \tag{7a}$$

$$\phi_E(0) = 0, \tag{7b}$$

$$V_E(0) = \sqrt{[\mu_S / r_E(0)]}, \tag{7c}$$

$$\gamma_E(0) = 0. \tag{7d}$$

3.2. Mars. In the Sun coordinate system, the Mars initial conditions ($t=0$) are written as

$$\text{(SCS)} \quad r_M(0) = \text{given}, \tag{8a}$$

$$\phi_M(0) = \text{free}, \tag{8b}$$

$$V_M(0) = \sqrt{[\mu_S / r_M(0)]}, \tag{8c}$$

$$\gamma_M(0) = 0. \tag{8d}$$

3.3. Spacecraft. In the Earth coordinate system, the spacecraft initial conditions ($t=0$) are given by

$$\text{(ECS)} \quad r_{PE}(0) = r_{LEO}, \tag{9a}$$

$$\phi_{PE}(0) = \text{free}, \tag{9b}$$

$$V_{PE}(0) = V_{LEO} + \Delta V_{LEO} = \sqrt{(\mu_E / r_{LEO})} + \Delta V_{LEO}, \tag{9c}$$

$$\gamma_{PE}(0) = 0. \tag{9d}$$

Relative to Earth r_{PE}, ϕ_{PE}, V_{PE}, γ_{PE} are the radial distance, phase angle, velocity, and path inclination of the spacecraft; V_{LEO} is the spacecraft velocity in the low Earth orbit prior to the application of the tangential velocity impulse; ΔV_{LEO} is the accelerating velocity impulse; V_{PE} is the spacecraft velocity after the application of the tangential velocity impulse. Note that the following inequalities must be satisfied at $t=0$:

$$\Delta V_{LEO} \geq (\sqrt{2}-1) V_{LEO} \rightarrowtail V_{PE} \geq \sqrt{2} V_{LEO}, \tag{9e}$$

if the spacecraft must leave near-Earth space toward deep interplanetary space.

4. Final Conditions

Let $t=\tau$ denote the final time. With this understanding, we state the final conditions for Earth, Mars, and spacecraft.

4.1. Earth. In the Sun coordinate system, the Earth final conditions ($t=\tau$) are given by

$$\text{(SCS)} \quad r_E(\tau) = r_E(0), \tag{10a}$$

$$\phi_E(\tau) = \tau\sqrt{[\mu_S / r_E^3(0)]}, \tag{10b}$$

$$V_E(\tau) = \sqrt{[\mu_S / r_E(0)]}, \tag{10c}$$

$$\gamma_E(\tau) = 0. \tag{10d}$$

4.2. Mars. In the Sun coordinate system, the Mars final conditions ($t=\tau$) are given by

$$\text{(SCS)} \quad r_M(\tau) = r_M(0), \tag{11a}$$

$$\phi_M(\tau) = \tau\sqrt{[\mu_S / r_M^3(0)]} + \phi_M(0), \tag{11b}$$

$$V_M(\tau) = \sqrt{[\mu_S / r_M(0)]}, \tag{11c}$$

$$\gamma_M(\tau) = 0. \tag{11d}$$

4.3. Spacecraft. In the Mars coordinate system, the spacecraft final conditions ($t=\tau$) are given by

$$\text{(MCS)} \quad r_{PM}(\tau) = r_{LMO} \tag{12a}$$

$$\phi_{PM}(\tau) = \text{free}, \tag{12b}$$

$$V_{PM}(\tau) = V_{LMO} + \Delta V_{LMO} = \sqrt{(\mu_M / r_{LMO})} + \Delta V_{LMO}, \tag{12c}$$

$$\gamma_{PM}(\tau) = 0. \tag{12d}$$

Relative to Mars r_{PM}, ϕ_{PM}, V_{PM}, γ_{PM} are the radial distance, phase angle, velocity, and path inclination of the spacecraft; V_{LMO} is the spacecraft velocity in the low Mars orbit after the application of the tangential velocity impulse; ΔV_{LMO} is the braking velocity impulse; V_{PM} is the spacecraft velocity before the application of the tangential velocity impulse. Note that the following inequalities must be satisfied at $t=\tau$:

$$\Delta V_{LMO} \geq (\sqrt{2}-1) V_{LMO} \rightarrowtail V_{PM} \geq \sqrt{2} V_{LMO}, \tag{12e}$$

if the spacecraft must enter near-Mars space from deep interplanetary space.

5. Coordinate System Transformation

In Sections 2–4, while the spacecraft differential equations are written in the Sun coordinate system (SCS), the spacecraft boundary conditions are

written in the Earth coordinate system (ECS) at departure from LEO and in the Mars coordinate system (MCS) at arrival on LMO. Therefore, it is important to develop general transformations allowing one to pass from Earth coordinates to Sun coordinates and back, and from Mars coordinates to Sun coordinates and back. For general information about coordinate system transformation, see Ref. 14.

Omitting details for brevity, we introduce the following vectors:

$$x_E = [r_E, \phi_E, V_E, \gamma_E]^T, \tag{13a}$$

$$x_M = [r_M, \phi_M, V_M, \gamma_M]^T, \tag{13b}$$

$$x_P = [r_P, \phi_P, V_P, \gamma_P]^T, \tag{13c}$$

$$x_{PE} = [r_{PE}, \phi_{PE}, V_{PE}, \gamma_{PE}]^T, \tag{13d}$$

$$x_{PM} = [r_{PM}, \phi_{PM}, V_{PM}, \gamma_{PM}]^T. \tag{13e}$$

ECS-to-SCS Transformation. Given the vectors x_E and x_{PE}, compute the vector x_P. This is achieved with the following relations:

$$r_P^2 = r_E^2 + r_{PE}^2 + 2r_E r_{PE} \cos \phi_{PE}, \tag{14a}$$

$$\phi_P = \arcsin[(r_E/r_P) \sin \phi_E + (r_{PE}/r_P) \sin(\phi_{PE} + \phi_E)], \quad \text{if } A \geq 0, \tag{14b}$$

$$\phi_P = \pi - \arcsin[(r_E/r_P) \sin \phi_E + (r_{PE}/r_P) \sin(\phi_{PE} + \phi_E)], \quad \text{if } A < 0, \tag{14b}$$

$$V_P^2 = V_E^2 + V_{PE}^2 + 2V_E V_{PE} \cos(\phi_{PE} - \gamma_{PE}), \tag{14c}$$

$$\gamma_P = -\arccos[(V_P^2 + V_E^2 - V_{PE}^2)/2V_P V_E] + \phi_P - \phi_E, \quad \text{if } B \geq 0, \tag{14d}$$

$$\gamma_P = \arccos[(V_P^2 + V_E^2 - V_{PE}^2)/2V_P V_E] + \phi_P - \phi_E, \quad \text{if } B < 0, \tag{14d}$$

where

$$A = r_E \cos \phi_E + r_{PE} \cos(\phi_{PE} + \phi_E), \tag{14e}$$

$$B = \phi_{PE} - \gamma_{PE}. \tag{14f}$$

SCS-to-ECS Transformation. Given the vectors x_E and x_P, compute the vector x_{PE}. This is achieved with the following relations:

$$r_{PE}^2 = r_P^2 + r_E^2 - 2r_P r_E \cos(\phi_P - \phi_E), \tag{15a}$$

$$\phi_{PE} = \arccos[-r_E/r_{PE} + (r_P/r_{PE}) \cos(\phi_P - \phi_E)], \quad \text{if } C \geq 0, \tag{15b}$$

$$\phi_{PE} = -\arccos[-r_E/r_{PE} + (r_P/r_{PE}) \cos(\phi_P - \phi_E)], \quad \text{if } C < 0, \tag{15b}$$

$$V_{PE}^2 = V_P^2 + V_E^2 - 2V_P V_E \cos(\phi_P - \phi_E - \gamma_P), \tag{15c}$$

$$\gamma_{PE} = \phi_{PE} - \arcsin[(V_P/V_{PE}) \sin(\phi_P - \phi_E - \gamma_P)], \quad \text{if } D \geq 0, \tag{15d}$$

$$\gamma_{PE} = \phi_{PE} - \pi + \arcsin[(V_P/V_{PE}) \sin(\phi_P - \phi_E - \gamma_P)], \quad \text{if } D < 0, \tag{15d}$$

where

$$C=\phi_P-\phi_E, \tag{15e}$$

$$D=V_P^2-V_E^2-V_{PE}^2. \tag{15f}$$

MCS-to-SCS Transformation. Given the vectors x_M and x_{PM}, compute the vector x_P. This is achieved with the following relations:

$$r_P^2 = r_M^2+r_{PM}^2+2r_M r_{PM}\cos\phi_{PM}, \tag{16a}$$

$$\phi_P = \arcsin[(r_M/r_P)\sin\phi_M+(r_{PM}/r_P)\sin(\phi_{PM}+\phi_M)], \quad \text{if } E\geq 0, \tag{16b}$$

$$\phi_P = \pi-\arcsin[(r_M/r_P)\sin\phi_M+(r_{PM}/r_P)\sin(\phi_{PM}+\phi_M)], \quad \text{if } E<0, \tag{16b}$$

$$V_P^2=V_M^2+V_{PM}^2+2V_M V_{PM}\cos(\phi_{PM}-\gamma_{PM}), \tag{16c}$$

$$\gamma_P = -\arccos[(V_P^2+V_M^2-V_{PM}^2)/2V_P V_M]+\phi_P-\phi_M, \quad \text{if } F\geq 0, \tag{16d}$$

$$\gamma_P = \arccos[(V_P^2+V_M^2-V_{PM}^2)/2V_P V_M]+\phi_P-\phi_M, \quad \text{if } F<0, \tag{16d}$$

where

$$E=r_M\cos\phi_M+r_{PM}\cos(\phi_{PM}+\phi_M), \tag{16e}$$

$$F=\phi_{PM}-\gamma_{PM}. \tag{16f}$$

SCS-to-MCS Transformation. Given the vectors x_M and x_P, compute the vector x_{PM}. This is achieved with the following relations:

$$r_{PM}^2 = r_P^2+r_M^2-2r_P r_M\cos(\phi_P-\phi_M), \tag{17a}$$

$$\phi_{PM} = \arccos[-r_M/r_{PM}+(r_P/r_{PM})\cos(\phi_P-\phi_M)], \quad \text{if } G\geq 0, \tag{17b}$$

$$\phi_{PM} = -\arccos[-r_M/r_{PM}+(r_P/r_{PM})\cos(\phi_P-\phi_M)], \quad \text{if } G<0, \tag{17b}$$

$$V_{PM}^2=V_P^2+V_M^2-2V_P V_M\cos(\phi_P-\phi_M-\gamma_P), \tag{17c}$$

$$\gamma_{PM} = \phi_{PM}-\arcsin[(V_P/V_{PM})\sin(\phi_P-\phi_M-\gamma_P)], \quad \text{if } H\geq 0, \tag{17d}$$

$$\gamma_{PM} = \phi_{PM}-\pi+\arcsin[(V_P/V_{PM})\sin(\phi_P-\phi_M-\gamma_P)], \quad \text{if } H<0, \tag{17d}$$

where

$$G=\phi_P-\phi_M, \tag{17e}$$

$$H=V_P^2-V_M^2-V_{PM}^2. \tag{17f}$$

6. Optimization Problem

We consider the Earth-to-Mars transfer of a spacecraft under the following conditions:

(B1) The spacecraft is initially in a low Earth orbit, flying with circular velocity $\sqrt{(\mu_E/r_{LEO})}$, with r_{LEO} given.

(B2) A tangential velocity impulse ΔV_{LEO} accelerates the spacecraft from circular velocity to hyperbolic velocity V_{PE} (relative to Earth) of sufficient magnitude so that the spacecraft escapes from near-Earth space into deep interplanetary space.

(B3) Subsequently, the spacecraft takes a long journey along an elliptic interplanetary orbit around Sun.

(B4) The spacecraft enters near-Mars space and reaches tangentially the low Mars orbit with hyperbolic velocity V_{PM} (relative to Mars).

(B5) A braking velocity impulse ΔV_{LMO} is applied tangentially so as to reduce the velocity relative to Mars from V_{PM} to the circular value $\sqrt{(\mu_M/r_{LMO})}$, with r_{LMO} given.

6.1. Performance Index. The most obvious performance index is the characteristic velocity

$$\Delta V = \Delta V_{LEO} + \Delta V_{LMO}, \tag{18}$$

which is the sum of the velocity impulses in low Earth orbit and low Mars orbit. The minimization of (18) is sought with respect to the vector function $x_P(t) = [r_P(t), \phi_P(t), V_P(t), \gamma_P(t)]^T$ satisfying the SCS differential constraints (5) on the time interval $0 \le t \le \tau$, the ECS initial conditions (9), and the MCS final conditions (12).

Note that minimizing ΔV is the same as minimizing the mass of propellant consumed, since this mass is a monotonically increasing function of ΔV.

6.2. Basic Parameters. Inspection of the differential constraints (5) and the initial conditions (9) shows that the computation of a particular trajectory forward in time requires the specification of the following parameter vector:

$$y = [\Delta V_{LEO}, \phi_{PE}(0), \phi_M(0), \tau]^T, \tag{19a}$$

where ΔV_{LEO} is the velocity impulse in low Earth orbit, $\phi_{PE}(0)$ is the initial phase angle of the spacecraft with respect to Earth, $\phi_M(0)$ is the initial phase angle of Mars with respect to Sun, and τ is the final time. Note that the

initial phase angle of Earth with respect to Sun is $\phi_E(0)=0$ by definition. Hence, $\phi_M(0)$ is the same as

$$\phi_M(0)=\phi_M(0)-\phi_E(0)=\Delta\phi(0), \tag{19b}$$

the initial planetary Mars/Earth phase angle difference with respect to Sun. Note that $\Delta\phi>0$ if Mars is ahead of Earth, $\Delta\phi=0$ if Mars and Earth are aligned with Sun, and $\Delta\phi<0$ if Mars is behind Earth. Also note that, in light of (19b), the parameter vector (19a) can be rewritten as

$$y=[\Delta V_{LEO},\ \phi_{PE}(0),\ \Delta\phi(0),\ \tau]^T. \tag{19c}$$

The arrival to a low Mars orbit must occur with a given radial distance from Mars and tangentially to LMO [see (12a) and (12d)],

$$r_{PM}(\tau)=r_{LMO}, \tag{20a}$$

$$\gamma_{PM}(\tau)=0. \tag{20b}$$

This means that a feasible trajectory is obtained if the parameter choice (19c) results in the satisfaction of (20). On the other hand, an optimal trajectory is obtained if, in addition to feasibility, one achieves the smallest value of the performance index (18).

6.3. Feasible Trajectory. A feasible trajectory can be computed through the following steps:

(C1) Assume that r_{LEO} is specified and the components of the parameter vector y [see (19c)] are given,

$$y=[\Delta V_{LEO},\ \phi_{PE}(0),\ \Delta\phi(0),\ \tau]^T. \tag{21a}$$

(C2) At the initial time $t=0$, use of Eqs. (9) shows that the vector $x_{PE}(0)$ is known,

$$x_{PE}(0)=[r_{PE}(0),\ \phi_{PE}(0),\ V_{PE}(0),\ \gamma_{PE}(0)]^T. \tag{21b}$$

(C3) Using the ECS-to-SCS transformation (14), obtain the vector

$$x_P(0)=[r_P(0),\ \phi_P(0),\ V_P(0),\ \gamma_P(0)]^T. \tag{21c}$$

(C4) Integrate the differential system (5) forward in time to obtain the vector function

$$x_P(t)=[r_P(t),\ \phi_P(t),\ V_P(t),\ \gamma_P(t)]^T, \tag{21d}$$

on the time interval $0\le t\le\tau$.

(C5) At the final time $t=\tau$, obtain the vector

$$x_P(\tau)=[r_P(\tau),\ \phi_P(\tau),\ V_P(\tau),\ \gamma_P(\tau)]^T. \tag{21e}$$

(C6) Using the SCS-to-MCS transformation (17), obtain the vector

$$x_{PM}(\tau)=[r_{PM}(\tau), \phi_{PM}(\tau), V_{PM}(\tau), \gamma_{PM}(\tau)]^T. \tag{21f}$$

(C7) At the final time $t=\tau$, check whether the vector (21f) is consistent with the MCS final conditions (12). Note that (12b) is irrelevant and that (12c) can be satisfied trivially via a proper choice of ΔV_{LMO}. Thus, we are left with (12a) and (12d), hence (20).

(C8) Defining the vector function

$$F(y)=[r_{PM}(\tau)-r_{LMO}, \gamma_{PM}(\tau)]^T, \tag{21g}$$

with $r_{PM}(\tau)$, $\gamma_{PM}(\tau)$ numerically related to the components of y via Steps C1–C7, it is clear that a feasible trajectory is obtained if the parameter choice (21a) results in $F(y)=0$, hence in the vanishing of the components of the vector function (21g).

(C9) If the choice of the vector y does not yield the zero of $F(y)$, then the components of y must be changed until $F(y)$ is brought to zero. This is in principle possible, since the feasible trajectory system has two degrees of freedom,

$$\dim y-\dim F(y)=4-2=2. \tag{21h}$$

The simplest way to implement Steps C1 through C9 is to employ the restoration algorithm component of the sequential gradient-restoration algorithm (SGRA) for mathematical programming problems (Refs. 15–16).

6.4. Optimal Trajectory. To compute an optimal trajectory, it is convenient to redefine the parameter vector y and the vector function $F(y)$ as follows:

$$y=[\Delta V_{LEO}, \phi_{PE}(0), \Delta\phi(0), \tau, \Delta V_{LMO}]^T, \tag{22a}$$

$$F(y)=[r_{PM}(\tau)-r_{LMO}, V_{PM}(\tau)-\sqrt{(\mu_M/r_{LMO})}-\Delta V_{LMO}, \gamma_{PM}(\tau)]^T, \tag{22b}$$

with $r_{PM}(\tau)$, $V_{PM}(\tau)$, $\gamma_{PM}(\tau)$ numerically related to the components of y via steps analogous to C1–C7. Note that the dimensions of y and $F(y)$ are increased by one, but that

$$\dim y-\dim F(y)=5-3=2. \tag{22c}$$

Once more, the feasible trajectory system has two degrees of freedom, which must be saturated in such a way that the minimum value of the performance index (18) is achieved. An algorithm suitable for this task is the sequential gradient-restoration algorithm (SGRA) for mathematical programming problems (Refs. 15–16). Details are omitted for brevity.

6.5. Comments on the Algorithm. The sequential gradient-restoration algorithm (SGRA) is an iterative technique which involves a sequence of two-phase cycles, each cycle including a gradient phase and a restoration phase. In the gradient phase, the augmented performance index (performance index augmented by the constraints weighted via appropriate Lagrange multipliers) is decreased, while avoiding excessive constraint violation. In the restoration phase, the constraint error is decreased, while avoiding excessive change in the performance index. In a complete gradient-restoration cycle, the performance index is decreased, while the constraints are satisfied to a preselected accuracy. Thus, a succession of feasible suboptimal solutions is generated, each new solution being an improvement over the previous one. SGRA is available in both mathematical programming format and optimal control format.

For mathematical programming problems, SGRA was developed by Miele et al. in both ordinary-gradient version and conjugate-gradient version (Ref. 15). Variations of SGRA were also developed, but the basic form proved to be the more reliable, because of its robustness and stability properties (Ref. 16).

For optimal control problems, the development of SGRA by Miele et al. (Refs. 17–22) has been parallel to that for mathematical programming problems. The resulting algorithm has proved to be a powerful tool for solving optimal trajectory problems of atmospheric and space flight (Refs. 23–26). Applications and extensions of SGRA have been reported in the US, Japan, Germany, and other countries around the world; in particular, a version of this algorithm is currently used at NASA-JSC under the code name SEGRAM, developed by McDonnell Douglas Technical Service Company (Ref. 26).

For the problem at hand (Earth-to-Mars optimal transfer), note that there are no control variables, only state variables and parameters. For this reason, it is preferable to use SGRA in mathematical programming format rather than optimal control format; either the ordinary gradient version or the conjugate gradient version can be used. Regardless of the version employed, the computation of gradients is much more complicated than in a standard mathematical programming problem.

6.6. Variable-Stepsize Integration Scheme. The optimization process requires multiple integrations of the system equations of the restricted four-body model. The integration process is computationally expensive and it is difficult to achieve the desired accuracy, owing to the fact that the total gravitational force changes rapidly in near-Earth and near-Mars space, but slowly in deep interplanetary space. Indeed, orbital periods are of order one hour to one day if Earth gravity or Mars gravity is dominant, but of order

one year if Sun gravity is dominant. The above difficulties can be overcome by properly designing a variable-stepsize integration scheme. Numerical experiments show that good results can be obtained by linking the integration stepsize to the total gravitational force, with the stepsize decreasing whenever the total gravitational force increases, and vice versa.

6.7. Computational Environment. The computations reported here are done on a Unix Sun Workstation using the C++ programming language. In particular, the integrations are done via a fifth-order Runge–Kutta–Fehlberg scheme. Double-precision arithmetic is used throughout the sequential gradient-restoration algorithm.

7. Planetary and Spacecraft Data

7.1. Planetary Data. Table 1 contains basic data relative to Earth, Mars, and Sun, namely: mass m, gravitational constant μ, surface radius

Table 1. Basic data on Sun, Earth, Mars.

Body	m [kg]	μ [km^3/s^2]	R [km]	H [km]
Sun	1.989E30	1.327E11	6.980E05	
Earth	5.976E24	3.986E05	6.378E03	120
Mars	6.418E23	4.283E04	3.397E03	100

m = mass, μ = gravitational constant, R = surface radius, H = atmospheric thickness.

Table 2. Orbital data on Earth and Mars.

Body	r [km]	V [km/s]	T [days]	ω [deg/day]
Earth	1.496E08	29.78	365	0.986
Mars	2.279E08	24.13	687	0.524

r = orbital radius, V = orbital velocity, T = orbital period, ω = angular velocity.

Table 3. Baseline terminal orbits for Mars mission.

Orbit	r [km]	h [km]	T [hrs]	V_c [km/s]	V_* [km/s]
LEO	6841	463	1.564	7.633	10.795
LMO	3597	200	1.819	3.451	4.880

r = orbital radius, h = orbital altitude, T = orbital period, V_c = circular velocity, V_* = escape velocity.

R, and atmospheric thickness H. In particular, note that the Sun mass is nearly 330,000 times the Earth mass and that the Earth mass is nearly 10 times the Mars mass; identical ratios hold for the gravitational constants.

Table 2 shows basic data relative to the orbits of Earth and Mars around Sun, namely: orbital radius r, orbital velocity V, orbital period T, and angular velocity ω. Vis-a-vis the Earth orbit, the Mars orbit has larger radius and period, but smaller translational velocity and angular velocity. In particular, the angular velocity difference between Earth and Mars is $\Delta\omega = 0.462$ deg/day; therefore, under the assumed model, Earth and Mars are in the same relative position every 779 days (every 2.13 years).

Table 3 contains data relative to the baseline terminal orbits employed in this study, namely: orbital radius r, orbital altitude h, orbital period T, circular velocity V_c, and escape velocity $V_* = \sqrt{2}V_c$. Vis-a-vis the low Mars orbit ($r_{LMO} = 3597$ km), the low Earth orbit ($r_{LEO} = 6841$ km) is characterized by much higher values of the circular velocity and escape velocity. From the table, it is easy to compute the following lower bounds for the accelerating velocity impulse at LEO, braking velocity impulse at LMO, and total characteristic velocity:

$$\Delta V_{LEO} \geq [V_* - V_c]_{LEO} = 3.162 \text{ km/s}, \tag{23a}$$

$$\Delta V_{LMO} \geq [V_* - V_c]_{LMO} = 1.429 \text{ km/s}, \tag{23b}$$

$$\Delta V \geq [V_* - V_c]_{LEO} + [V_* - V_c]_{LMO} = 4.591 \text{ km/s}. \tag{23c}$$

7.2. Spacecraft Data. The spacecraft is to be launched from LEO. Relative to Earth, the initial radial distance is $r_{PE}(0) = 6841$ km, corresponding to the altitude $h_{PE}(0) = 463$ km, close to that of the space station. Relative to Earth, the initial path inclination is $\gamma_{PE}(0) = 0$ deg. Because of the lower bound (23a) on the velocity impulse at LEO, the spacecraft velocity after application of the velocity impulse must satisfy the lower bound

$$V_{PE}(0) = V_{LEO} + \Delta V_{LEO} \geq [V_*]_{LEO} = 10.795 \text{ km/s}. \tag{24a}$$

The initial phase angle of the spacecraft with respect to Earth $\phi_{PE}(0)$ is free and must be determined via optimal trajectory computation together with the velocity impulse ΔV_{LEO} and the planetary Mars/Earth phase angle difference $\Delta\phi(0)$.

Following the interplanetary journey, the spacecraft arrives at LMO. Relative to Mars, the final radial distance is $r_{PM}(\tau) = 3597$ km, corresponding to the altitude $h_{PM}(\tau) = 200$ km. Relative to Mars, the final path inclination is $\gamma_{PM}(\tau) = 0$ deg. Because of the lower bound (23b) on the velocity impulse at LMO, the spacecraft velocity before the application of the velocity

impulse must satisfy the lower bound

$$V_{PM}(\tau) = V_{LMO} + \Delta V_{LMO} \geq [V_*]_{LMO} = 4.880 \text{ km/s}. \tag{24b}$$

The final phase angle of the spacecraft with respect to Mars $\phi_{PM}(\tau)$ is free and must be determined via optimal trajectory computation together with the final time τ, velocity impulse ΔV_{LMO}, and planetary Mars/Earth phase angle difference $\Delta\phi(\tau)$.

It must be emphasized that the lower bounds (23)–(24) hold specifically for the baseline terminal radii of Table 3. Should the terminal radii change, the lower bounds in (23)–(24) would change.

8. Baseline Optimal Trajectory

Problem P1 deals with the determination of the optimal LEO-to-LMO transfer for given LEO and LMO radii, specifically,

$$r_{LEO} = 6841 \text{ km}, \qquad r_{LMO} = 3597 \text{ km}, \tag{25a}$$

corresponding to the terminal altitudes

$$h_{LEO} = 463 \text{ km}, \qquad h_{LMO} = 200 \text{ km}. \tag{25b}$$

For this problem, the feasible trajectory system has two degrees of freedom, to be saturated by minimizing the total characteristic velocity (18).

8.1. Results. The sequential gradient-restoration algorithm for mathematical programming problems was employed to solve Problem P1. Summary results are shown qualitatively in Figs. 1–3 and quantitatively in Tables 4–5.

Figure 1 refers to deep interplanetary space and shows the complete trajectories of Earth, Mars, and spacecraft. Figure 2 refers to near-Earth space and highlights the initial part of the spacecraft trajectory in Earth coordinates. Figure 3 refers to near-Mars space and highlights the final part of the spacecraft trajectory in Mars coordinates.

Tables 4–5 present the values of the state variables for Earth, Mars, and spacecraft at departure from LEO and at arrival on LMO; Sun coordinates are used for Earth and Mars; Sun, Earth, and Mars coordinates are used for spacecraft. Main comments are as follows:

(i) Relative to Earth, the spacecraft leaves the low Earth orbit tangentially with an initial velocity impulse $\Delta V_{LEO} = 3.552$ km/s and an initial phase angle $\phi_{PE}(0) = -61.85$ deg, meaning that the accelerating velocity impulse is applied 61.85 deg before the spacecraft becomes aligned with the Earth and Sun centers. Relative to Sun, the planetary Mars/Earth phase

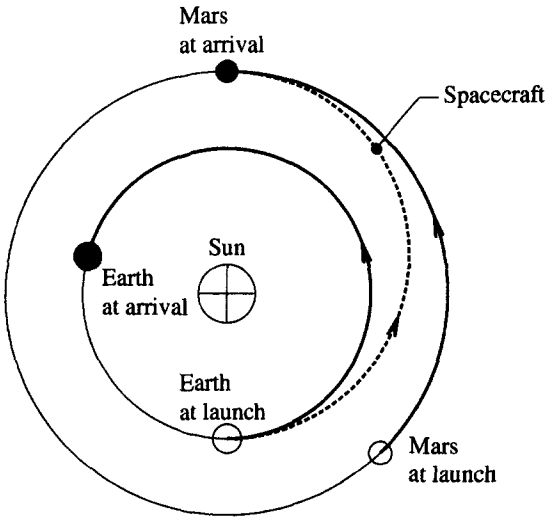

Fig. 1. Spacecraft trajectory, deep interplanetary space, Sun coordinate system.

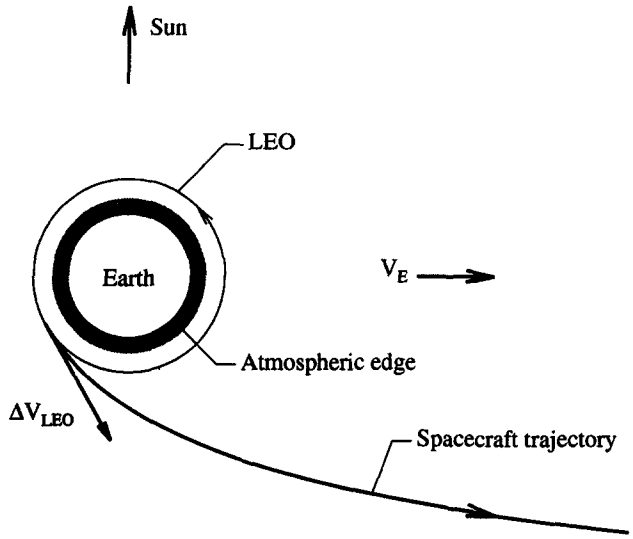

Fig. 2. Spacecraft trajectory, near-Earth space, Earth coordinate system.

angle difference is $\Delta\phi(0) = +43.86$ deg, meaning that Mars is ahead of Earth by 43.86 deg at departure.

(ii) Relative to Mars, the spacecraft reaches the low Mars orbit tangentially with a final velocity impulse $\Delta V_{LMO} = 2.100$ km/s and a final phase

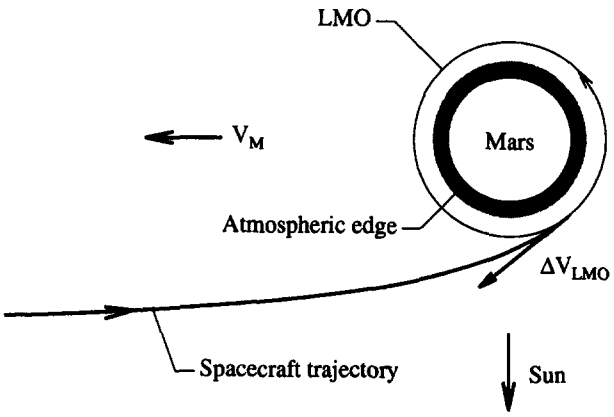

Fig. 3. Spacecraft trajectory, near-Mars space, Mars coordinate system.

angle $\phi_{PM}(\tau) = -140.97$ deg, meaning that the braking velocity impulse is applied 140.97 deg before the spacecraft becomes aligned with the Mars and Sun centers. Relative to Sun, the planetary Mars/Earth phase angle difference is $\Delta\phi(\tau) = -75.13$ deg, meaning that Mars is behind Earth by 75.13 deg at arrival.

(iii) The total characteristic velocity is $\Delta V = 5.652$ km/s and the transfer time is $\tau = 257.88$ days. During this time, the angular travel of the

Table 4. Baseline optimal trajectory: Inertial and relative state variables at $t = 0$.

Body	System	Subscript	r [km]	ϕ [deg]	V [km/s]	γ [deg]
Earth	SCS	E	1.496E08	0.00	29.78	0.00
Mars	SCS	M	2.279E08	43.86	24.13	0.00
Spacecraft	SCS	P	1.496E08	0.00	36.42	15.71
Spacecraft	ECS	PE	6.841E03	−61.85	11.19	0.00
Spacecraft	MCS	PM	1.586E08	−139.19	31.91	−38.93

$\Delta V_{LEO} = 3.552$ km/s, $\phi_{PE}(0) = -61.85$ deg, $\Delta\phi(0) = +43.86$ deg.

Table 5. Baseline optimal trajectory: Inertial and relative state variables at $t = \tau$.

Body	System	Subscript	r [km]	ϕ [deg]	V [km/s]	γ [deg]
Earth	SCS	E	1.496E08	254.15	29.78	0.00
Mars	SCS	M	2.279E08	179.02	24.13	0.00
Spacecraft	SCS	P	2.279E08	179.02	20.13	10.02
Spacecraft	ECS	PE	2.384E03	−112.47	34.50	31.99
Spacecraft	MCS	PM	3.597E08	−140.97	5.55	0.00

$\Delta V_{LMO} = 2.100$ km/s, $\phi_{PM}(\tau) = -140.97$ deg, $\Delta\phi(\tau) = -75.13$ deg, $\tau = 257.88$ days.

spacecraft around Sun is 179.02 deg, to be compared with 254.15 deg for Earth and 135.16 deg for Mars.

9. Departure Window

For given LEO and LMO radii [see (25)], Problem P2 deals with the computation of a one-parameter family of suboptimal transfers, obtained by changing the planetary Mars/Earth phase angle difference $\Delta\phi(0)$, hence changing the departure date θ vis-a-vis the optimal value determined by solving Problem P1. While the feasible trajectory system of Problem P1 has two degrees of freedom, that of Problem P2 has one degree of freedom, resulting in an increase in total characteristic velocity (18). To contain this increase, we reoptimize the trajectory; that is, for each preselected value of $\Delta\phi(0)$, we determine the new optimal values of the remaining components of the vector parameter y [see (22a)].

The following relation holds between the changes in planetary Mars/Earth phase angle difference and departure date:

$$[\Delta\phi(0)]_{P2} - [\Delta\phi(0)]_{P1} + (\theta_{P2} - \theta_{P1})\Delta\omega = 0, \tag{26}$$

where $\Delta\omega = 0.462$ deg/day is the angular velocity difference between Earth and Mars. Clearly, the results of Problem P2 can be parametrized in terms of either $\Delta\phi(0)$ or $\Delta\theta$, with $\Delta\theta = \theta_{P2} - \theta_{P1}$ and the following understanding: larger values of $\Delta\phi(0)$ denote early departure, $\Delta\theta < 0$; conversely, smaller value of $\Delta\phi(0)$ denote delayed departure, $\Delta\theta > 0$.

9.1. Remark. Departure window studies are important for the following reason. They help determining the tolerance in departure date compatible with the requirements of an Earth-to-Mars mission. If launch cannot be executed within a reasonable period of time around an optimal departure date, there is a heavy penalty associated with long postponment: the next favorable launch condition occurs 779 days later [360 deg/(0.462 deg/day)], hence 2.13 years later.

9.2. Results. The sequential gradient-restoration algorithm for mathematical programming problem was employed to solve Problem P2 for several values of $\Delta\phi(0)$, hence several values of $\Delta\theta$. Summary results are shown in Figs. 4–12 and Tables 6–8.

Figures 4–6 present inertial values of the spacecraft state variables at departure and arrival; Sun coordinates are used. For more precise values, see Tables 6–7.

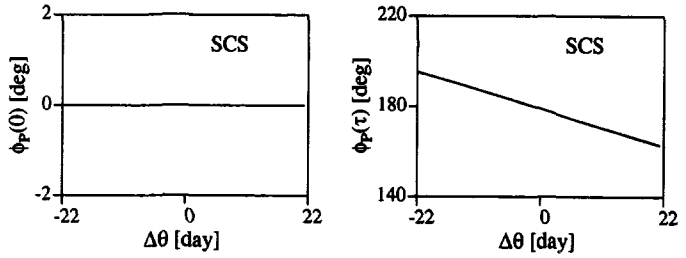

Fig. 4. Departure window: Spacecraft inertial phase angle at $t=0$ and $t=\tau$.

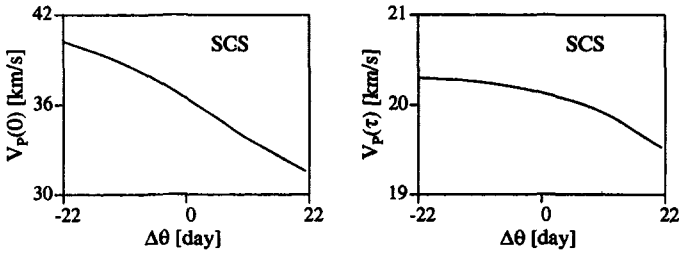

Fig. 5. Departure window: Spacecraft inertial velocity at $t=0$ and $t=\tau$.

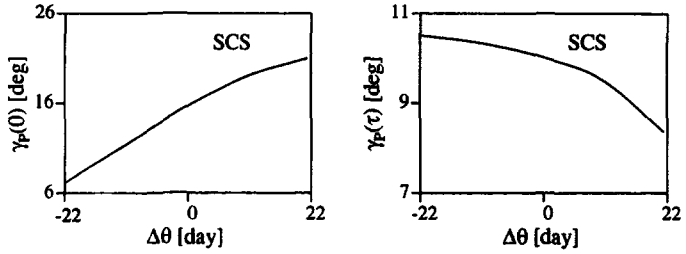

Fig. 6. Departure window: Spacecraft inertial path inclination at $t=0$ and $t=\tau$.

Figures 7–9 present relative values of the spacecraft state variables at departure and arrival; Earth coordinates are used at departure and Mars coordinates are used at arrival. For more precise values, see Tables 6–7.

Figures 10–12 present the planetary Mars/Earth phase angle difference at departure and arrival (Fig. 10), characteristic velocity components at departure and arrival (Fig. 11), as well as total characteristic velocity and transfer time (Fig. 12). For more precise values, see Table 8. Main comments are as follows:

(i) A change in departure date of ∓ 22 days causes a change in planetary Mars/Earth phase angle difference at departure of ± 10 deg; at arrival, the planetary Mars/Earth phase angle difference changes by ± 5 deg.

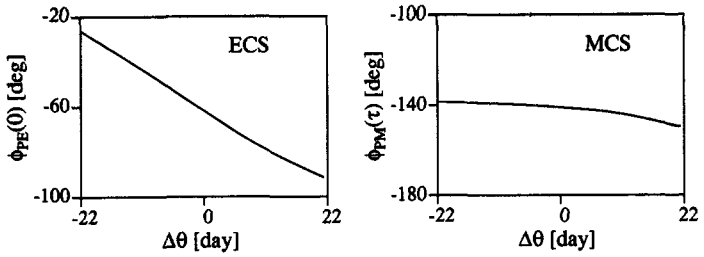

Fig. 7. Departure window: Spacecraft relative phase angle at $t=0$ and $t=\tau$.

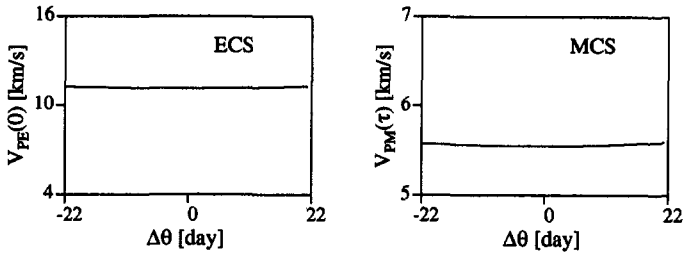

Fig. 8. Departure window: Spacecraft relative velocity at $t=0$ and $t=\tau$.

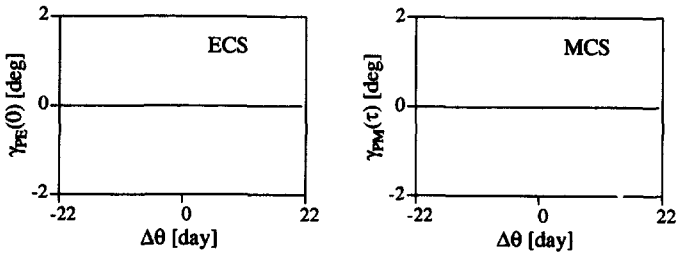

Fig. 9. Departure window: Spacecraft relative path inclination at $t=0$ and $t=\tau$.

(ii) A change in departure date of ∓ 22 days causes a relative increase in total characteristic velocity of 2.5 percent for early departure and 3.4 percent for late departure.

(iii) A change in departure date of ∓ 22 days causes a change in flight time of ± 12 days.

(iv) A change in departure date of ∓ 22 days causes a change of spacecraft phase angle relative to Earth $\phi_{PE}(0)$ of $+35$ deg for early departure and -30 deg for late departure. This is compensated by a change in the spacecraft inertial velocity $V_P(0)$ [velocity with respect to Sun] of $+3.8$ km/s for early departure and -4.9 km/s for late departure.

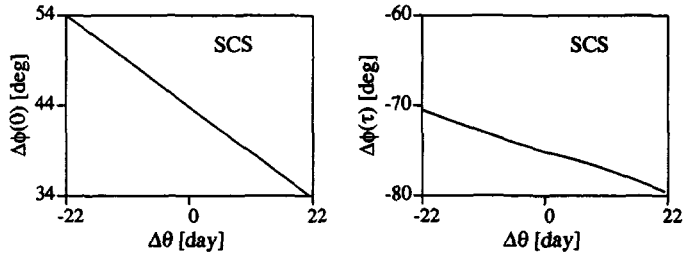

Fig. 10. Departure window: Planetary Mars/Earth phase angle difference at $t=0$ and $t=\tau$.

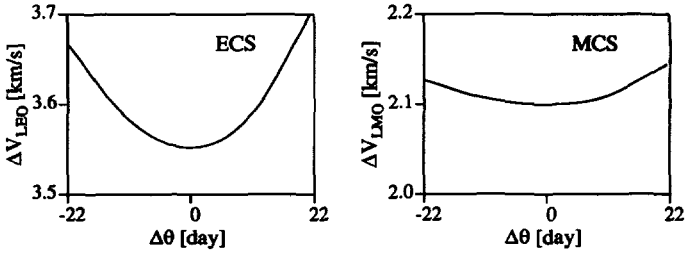

Fig. 11. Departure window: Characteristic velocity components at $t=0$ and $t=\tau$.

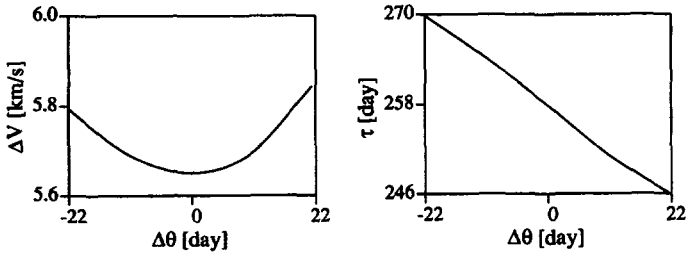

Fig. 12. Departure window: Total characteristic velocity and transfer time.

10. Arrival Window

For given LEO radius [see (25a)], Problem P3 deals with the computation of a one-parameter family of optimal transfers, obtained by changing the LMO radius. For each preselected value of r_{LMO}, Problem P3 is mathematically the same as Problem P1 in that the feasible trajectory system has two degrees of freedom, to be saturated in such a way that the total characteristic velocity ΔV [see (18)] is minimized. Once more, the optimal values of the components of the vector parameter y [see (22a)] are to be determined.

Table 6. Departure window: Inertial and relative state variables at $t=0$.

$\Delta\theta$	−21.99	−11.15	0.00	10.52	21.36	day
$r_P(0)$	1.496E08	1.496E08	1.496E08	1.496E08	1.496E08	km
$\phi_P(0)$	0.00	0.00	0.00	0.00	0.00	deg
$V_P(0)$	40.22	38.73	36.42	33.85	31.57	km/s
$\gamma_P(0)$	7.17	11.42	15.71	18.95	21.03	deg
$r_{PE}(0)$	6.841E03	6.841E03	6.841E03	6.841E03	6.841E03	km
$\phi_{PE}(0)$	−26.36	−43.14	−61.85	−78.51	−91.60	deg
$V_{PE}(0)$	11.30	11.22	11.19	11.22	11.33	km/s
$\gamma_{PE}(0)$	0.00	0.00	0.00	0.00	0.00	deg

Table 7. Departure window: Inertial and relative state variables at $t=\tau$.

$\Delta\theta$	−21.99	−11.15	0.00	10.52	21.36	day
$r_P(\tau)$	2.279E08	2.279E08	2.279E08	2.279E08	2.279E08	km
$\phi_P(\tau)$	195.41	187.51	179.02	170.74	162.99	deg
$V_P(\tau)$	20.30	20.25	20.13	19.93	19.52	km/s
$\gamma_P(\tau)$	10.51	10.34	10.02	9.52	8.37	deg
$r_{PM}(\tau)$	3.597E03	3.597E03	3.597E03	3.597E03	3.597E03	km
$\phi_{PM}(\tau)$	−138.50	−139.26	−140.97	−143.73	−149.56	deg
$V_{PM}(\tau)$	5.58	5.56	5.55	5.56	5.60	km/s
$\gamma_{PM}(\tau)$	0.00	0.00	0.00	0.00	0.00	deg

Table 8. Departure window: Planetary Mars/Earth phase angle differences, characteristic velocities, and transfer time.

$\Delta\theta$	−21.99	−11.15	0.00	10.52	21.36	day
$\Delta\phi(0)$	54.00	49.00	43.86	39.00	34.00	deg
$\Delta\phi(\tau)$	−70.48	−72.93	−75.13	−76.97	−79.55	deg
ΔV_{LEO}	3.667	3.583	3.552	3.587	3.701	km/s
ΔV_{LMO}	2.127	2.107	2.100	2.109	2.144	km/s
ΔV	5.794	5.690	5.652	5.695	5.844	km/s
τ	269.79	264.26	257.88	251.35	246.10	day

10.1. Results. The sequential gradient-restoration algorithm for mathematical programming problems was employed to solve Problem P3 for several values of r_{LMO}. Summary results are shown in Figs. 13–21 and Tables 9–11.

Figures 13–15 present inertial values of the spacecraft state variables at departure and arrival; Sun coordinates are used. For more precise values, see Tables 9–10.

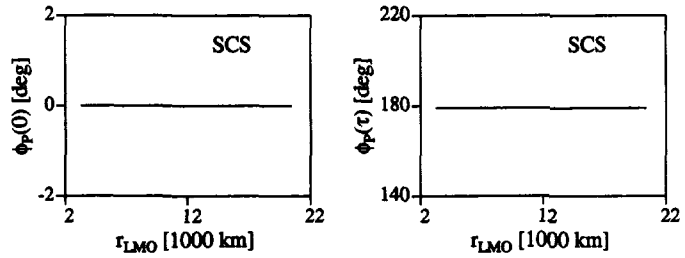

Fig. 13. Arrival window: Spacecraft inertial phase angle at $t=0$ and $t=\tau$.

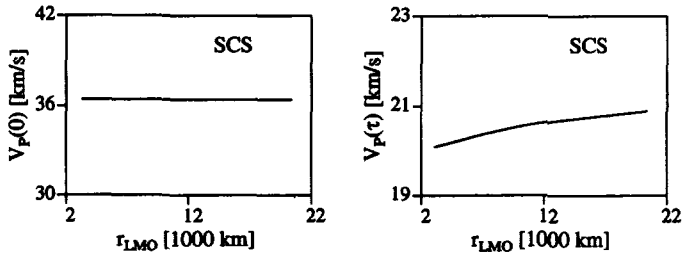

Fig. 14. Arrival window: Spacecraft inertial velocity at $t=0$ and $t=\tau$.

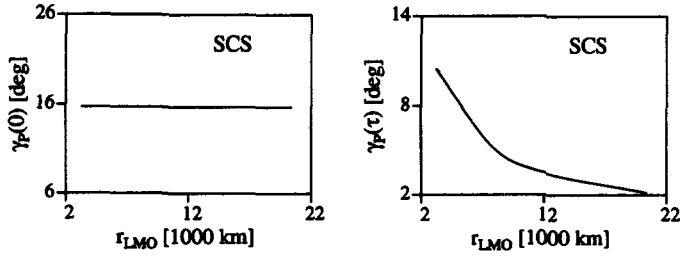

Fig. 15. Arrival window: Spacecraft inertial path inclination at $t=0$ and $t=\tau$.

Figures 16–18 present relative values of the spacecraft state variables at departure and arrival; Earth coordinates are used at departure and Mars coordinates are used at arrival. For more precise values, see Tables 9–10.

Figures 19–21 present the planetary Mars/Earth phase angle difference at departure and arrival (Fig. 19), characteristic velocity components at departure and arrival (Fig. 20), as well as total characteristic velocity and transfer time (Fig. 21). For more precise values, see Table 11. Main comments are as follows:

(i) The LMO radii considered range from 3467 to 20,415 km, corresponding to altitudes from 70 to 17,018 km.

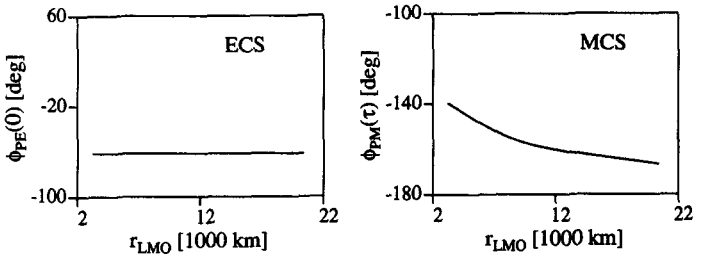

Fig. 16. Arrival window: Spacecraft relative phase angle at $t=0$ and $t=\tau$.

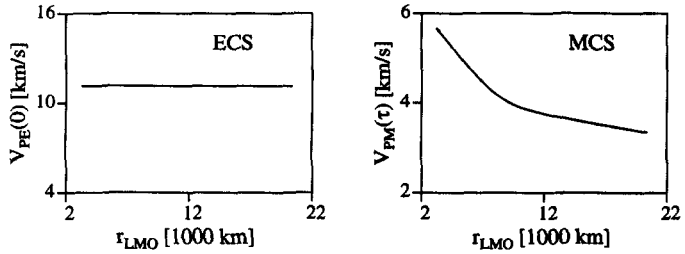

Fig. 17. Arrival window: Spacecraft relative velocity at $t=0$ and $t=\tau$.

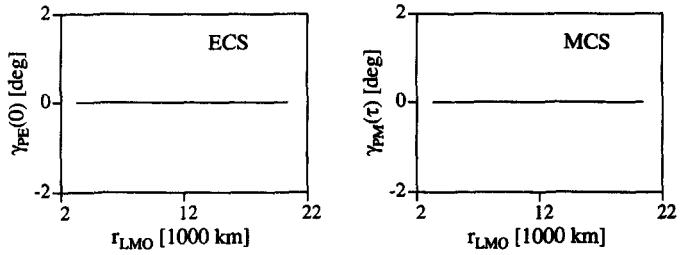

Fig. 18. Arrival window: Spacecraft relative path inclination at $t=0$ and $t=\tau$.

(ii) Each numerical column in Tables 9–11 represents a different solution of Problem P3; in particular, Column 1 characterizes an orbit inside the upper Mars atmosphere; Column 2 is the same as the solution of Problem P1; Column 5 characterizes a Mars-synchronous orbit.

(iii) Generally speaking, the state variables at departure are nearly independent of the radius of the Mars orbit: as r_{LMO} varies, they change in at most the third or fourth significant figure (Table 9); however, the state variables at arrival exhibit larger changes (Table 10).

(iv) As r_{LMO} changes, the planetary Mars/Earth phase angle difference at departure $\Delta\phi(0)$ changes in at most the fourth significant figure; the

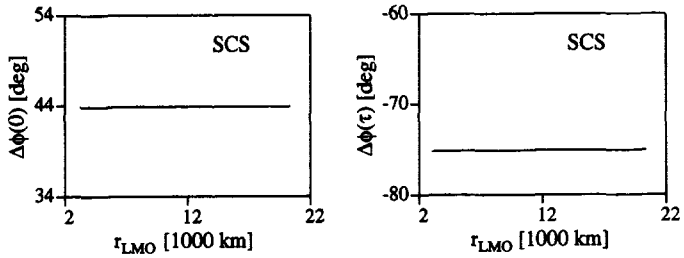

Fig. 19. Arrival window: Planetary Mars/Earth phase angle difference at $t=0$ and $t=\tau$.

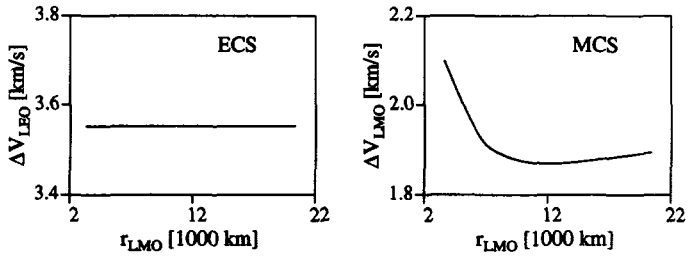

Fig. 20. Arrival window: Characteristic velocity components at $t=0$ and $t=\tau$.

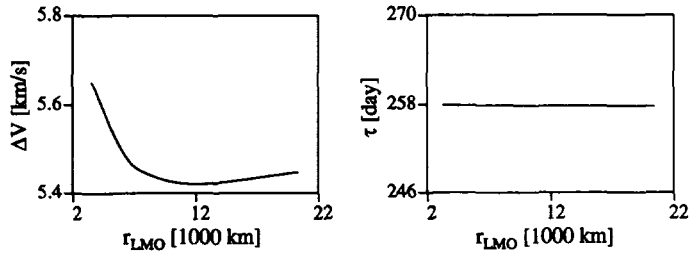

Fig. 21. Arrival window: Total characteristic velocity and transfer time.

analogous quantity at arrival $\Delta\phi(\tau)$ changes in at most the third significant figure (Table 11).

(v) As r_{LMO} varies, the total characteristic velocity ΔV changes in at most the second significant figure. Indeed, ΔV decreases with r_{LMO} near the Mars surface and increases with r_{LMO} far away from the Mars surface, exhibiting a minimum value $\Delta V = 5.421$ km/s at $r_{LMO} = 12{,}277$ km (Column 4 of Table 11); this is 4.3 percent below the value $\Delta V = 5.667$ km/s occurring for $r_{LMO} = 3467$ km (Column 1) and 0.5 percent below the value $\Delta V = 5.447$ km/s occurring for $r_{LMO} = 20{,}415$ km (Column 5).

Table 9. Arrival window: Inertial and relative state variables at $t=0$.

r_{LMO}	3467	3597	8000	12,277	20,415	km
h_{LMO}	70	200	4603	8880	17,018	km
$r_P(0)$	1.496E08	1.496E08	1.496E08	1.496E08	1.496E08	km
$\phi_P(0)$	0.00	0.00	0.00	0.00	0.00	deg
$V_P(0)$	36.42	36.42	36.42	36.42	36.42	km/s
$\gamma_P(0)$	15.71	15.71	15.71	15.71	15.71	deg
$r_{PE}(0)$	6.841E03	6.841E03	6.841E03	6.841E03	6.841E03	km
$\phi_{PE}(0)$	−61.85	−61.85	−61.85	−61.85	−61.86	deg
$V_{PE}(0)$	11.19	11.19	11.19	11.19	11.19	km/s
$\gamma_{PE}(0)$	0.00	0.00	0.00	0.00	0.00	deg

Table 10. Arrival window: Inertial and relative state variables at $t=\tau$.

r_{LMO}	3467	3597	8000	12,277	20,415	km
h_{LMO}	70	200	4603	8880	17,018	km
$r_P(\tau)$	2.279E08	2.279E08	2.279E08	2.279E08	2.279E08	km
$\phi_P(\tau)$	179.02	179.02	179.01	178.97	178.96	deg
$V_P(\tau)$	20.13	20.13	20.43	20.65	20.90	km/s
$\gamma_P(\tau)$	10.31	10.02	5.14	3.49	2.15	deg
$r_{PM}(\tau)$	3.467E03	3.597E03	8.000E03	1.228E04	2.042E04	km
$\phi_{PM}(\tau)$	−140.32	−140.97	−154.29	−160.44	−166.52	deg
$V_{PM}(\tau)$	5.63	5.55	4.21	3.74	3.34	km/s
$\gamma_{PM}(\tau)$	0.00	0.00	0.00	0.00	0.00	deg

Table 11. Arrival window: Planetary Mars/Earth phase angle differences, characteristic velocities, and transfer time.

r_{LMO}	3467	3597	8000	12,277	20,415	km
h_{LMO}	70	200	4603	8880	17,018	km
$\Delta\phi(0)$	43.86	43.86	43.86	43.87	43.87	deg
$\Delta\phi(\tau)$	−75.12	−75.13	−75.11	−75.05	−75.04	deg
ΔV_{LEO}	3.552	3.552	3.552	3.552	3.552	km/s
ΔV_{LMO}	2.115	2.100	1.893	1.869	1.895	km/s
ΔV	5.667	5.652	5.445	5.421	5.447	km/s
τ	257.86	257.88	257.85	257.75	257.73	day

(vi) As r_{LMO} varies, the transfer time τ changes in at most the fourth significant figure (Table 11).

(vii) With reference to (v), note that the period associated with a radius of 12,277 km is 11.5 hours, which is slightly less than half the Mars-synchronous period of 24.6 hours, associated with a radius of 20,415 km.

10.2. Guidance Implications. The main observation arising from the study of Problem P3 is that the conditions at departure are almost independent of r_{LMO}. On the other hand, this is not the case with the conditions at arrival; in particular the velocity and path inclination change considerably in near-Mars space owing to gravitational effects. These results have important implications for guidance. They mean that one can use the same launch conditions regardless of the desired orbital radius at Mars; a midcourse correction (velocity impulse) is all that is needed to ensure that a specified orbital radius is achieved at arrival.

11. Optimum–Optimorum Trajectory

Problem P4 arises from Problem P3 by regarding the arrival radius r_{LMO} as a variable; for given r_{LEO} [see (25a)], the minimization of ΔV is done with respect to both the components of the vector parameter y [see (22a)] and the scalar r_{LMO}. Under this scenario, the feasible trajectory system has three degrees of freedom, to be saturated in such a way that the total characteristic velocity ΔV [see (18)] is minimized.

The resulting trajectory is called optimum-optimorum trajectory in that it yields the smallest characteristic velocity compatible with the chosen departure radius $r_{LEO} = 6841$ km, corresponding to the altitude $h_{LEO} = 463$ km. The optimal value of the arrival radius is $r_{LMO} = 12{,}277$ km, corresponding to the altitude $h = 8880$ km. At this altitude, the orbital period is 11.5 hours; this is slightly less than half the Mars-synchronous period at 24.6 hours associated with a radius of 20,415 km. Summary results are presented in Column 4 of Tables 9–11. For more detailed information, see Tables 12–13.

12. Conclusions

From the analysis made, the following conclusions emerge for a spacecraft being transferred from a low Earth orbit to a low Mars orbit.

Table 12. Optimum–optimorum trajectory: Inertial and relative state variables at $t = 0$.

Body	System	Subscript	r [km]	ϕ [deg]	V [km/s]	γ [deg]
Earth	SCS	E	1.496E08	0.00	29.78	0.00
Mars	SCS	M	2.279E08	43.87	24.13	0.00
Spacecraft	SCS	P	1.496E08	0.00	36.42	15.71
Spacecraft	ECS	PE	6.841E03	−61.85	11.19	0.00
Spacecraft	MCS	PM	1.586E08	−139.19	31.92	−38.92

$\Delta V_{LEO} = 3.552$ km/s, $\phi_{PE}(0) = -61.85$ deg, $\Delta\phi(0) = +43.87$ deg.

Table 13. Optimum-optimorum trajectory: Inertial and relative state variables at $t=\tau$.

Body	System	Subscript	r [km]	ϕ [deg]	V [km/s]	γ [deg]
Earth	SCS	E	1.496E08	254.02	29.78	0.00
Mars	SCS	M	2.279E08	178.97	24.13	0.00
Spacecraft	SCS	P	2.279E08	178.97	20.65	3.49
Spacecraft	ECS	PE	2.382E03	−112.41	32.69	29.34
Spacecraft	MCS	PM	1.228E04	−160.44	3.74	0.00

$\Delta V_{LMO}=1.869$ km/s, $\phi_{PM}(\tau)=-160.44$ deg, $\Delta\phi(\tau)=-75.05$ deg, $\tau=257.75$ days.

(i) Baseline Optimal trajectory. The spacecraft leaves the low Earth orbit ($h_{LEO}=463$ km) with an accelerating velocity impulse $\Delta V_{LEO}=3.552$ km/s, phase angle relative to Earth $\phi_{PE}(0)=-61.85$ deg, and planetary Mars/Earth phase angle difference $\Delta\phi(0)=+43.86$ deg. The spacecraft reaches the low Mars orbit ($h_{LMO}=200$ km) with a braking velocity impulse $\Delta V_{LMO}=2.100$ km/s, phase angle relative to Mars $\phi_{PM}(\tau)=-140.97$ deg, and planetary Mars/Earth phase angle difference $\Delta\phi(\tau)=-75.13$ deg. The total characteristic velocity is $\Delta V=5.652$ km/s and the transfer time is $\tau=257.88$ days. During this time, the angular travel of the spacecraft with respect to Sun is 179.02 deg, to be compared with 254.15 deg for Earth and 135.16 deg for Mars.

(ii) Departure Window. If a spacecraft cannot be launched at the correct departure date, hence at the correct planetary Mars/Earth phase angle difference, the total characteristic velocity increases. To contain this increase, a one-parameter family of suboptimal trajectories has been computed, with the following implications: a change in departure date of ∓ 22 days causes a change in planetary Mars/Earth phase angle difference at departure $\Delta(\Delta\phi(0))$ of ± 10 deg and a change of spacecraft phase angle relative to Earth $\Delta\phi_{PE}(0)$ of $+35$ deg for early departure and -30 deg for late departure; this results in a flight time change $\Delta\tau$ of ± 12 days, a change in planetary Mars/Earth phase angle difference at arrival $\Delta(\Delta\phi(\tau))$ of ± 5 deg, and a relative increase in total characteristic velocity of 2.5 percent for early departure and 3.4 percent for late departure.

(iii) Arrival Window. A one-parameter family of optimal trajectories can be generated by changing the radius of the low Mars orbit, while keeping constant the radius of the low Earth orbit. The analysis shows that the departure conditions remain almost unchanged, while this is not the case with the arrival conditions; see in particular the values of velocity and path inclination at arrival. This result has important implications for guidance: it means that, for the same initial conditions, one can achieve different final

conditions (in particular, different final radii r_{LMO}) by means of a midcourse correction to the spacecraft velocity.

(iv) Optimum–Optimorum Trajectory. Among the members of the above one-parameter family, there is a trajectory with the smallest characteristic velocity. This occurs for $r_{LMO} = 12{,}277$ km, corresponding to $h_{LMO} = 8800$ km. At this altitude, the orbital period is 11.5 hours, which is slightly less than half the Mars-synchronous period of 24.6 hours. The total characteristic velocity of the optimum-optimorum trajectory $\Delta V = 5.421$ km/s is 4.1 percent lower than the total characteristic velocity $\Delta V = 5.652$ km/s of the baseline optimal trajectory.

Extensions of the present analysis are under way to increase the amplitude of the θ range, hence the amplitude of the $\Delta\phi(0)$ range, covered by the departure window. Further extensions are under way to include the ellipticity of the motion of Earth and Mars plus the fact that the Earth and Mars orbital planes are not identical.

References

1. ANONYMOUS, *The Viking Mission to Mars*, Martin Marietta Corporation, Denver, Colorado, 1975.
2. LECOMPTE, M., *New Approaches to Space Exploration*, The Case for Mars, Edited by P. J. Boston, Univelt, San Diego, California, pp. 35–37, 1984.
3. NIEHOFF, J. C., *Pathways to Mars: New Trajectory Opportunities*, NASA Mars Conference, Edited by D. B. Reiber, Univelt, San Diego, California, pp. 381–401, 1988.
4. WERCINSKI, P. F., *Mars Sample Return: A Direct and Minimum-Risk Design*, Journal of Spacecraft and Rockets, Vol. 33, No. 3, pp. 381–385, 1996.
5. LINDORFER, W., and MOYER, H. G., *Application of a Low Thrust Trajectory Optimization Scheme to Planar Earth-Mars Transfer*, ARS Journal, Vol. 32, pp. 260–262, 1962.
6. STRIEP, S. A., BRAUN, R. D., POWELL, R. W., and FOWLER, W. T., *Influence of Interplanetary Trajectory Selection on Mars Atmospheric Entry Velocity*, Journal of Spacecraft and Rockets, Vol. 30, No. 4, pp. 26–430, 1993.
7. TAUBER, M., HENLINE, W., CHARGIN, M., PAPADOPOULOS, P., CHEN, Y., YANG, L., and HAMM, K., *Mars Environmental Survey Probe, Aerobrake Preliminary Design Study*, Journal of Spacecraft and Rockets, Vol. 30, No. 4, pp. 431–437, 1993.
8. BRAUN, R. D., POWELL, R. W., ENGELUND, W. C., GNOFFO, P. A., WEILMUENSTER, K. J., and MITCHELTREE, R. A., *Mars Pathfinder Six-Degree-of-Freedom Entry Analysis*, Journal of Spacecraft and Rockets, Vol. 32, No. 6, pp. 993–1000, 1995.
9. PASTRONE, D., CASALINO, L., and COLASURDO, G., *Indirect Optimization Method for Round-Trip Mars Trajectories*, Astrodynamics 1995, Edited by K. T.

Alfriend, I. M. Ross, A. K. Misra, and C. F. Peters, Univelt, San Diego, California, pp. 85–99, 1995.

10. SPENCER, D. A., and BRAUN, R. D., *Mars Pathfinder Atmospheric Entry: Trajectory Design and Dispersion Analysis,* Journal of Spacecraft and Rockets, Vol. 33, No. 5, pp. 670–676, 1996.
11. LEE, W., and SIDNEY, W., *Mission Plan for Mars Global Surveyor*, Spaceflight Mechanics 1996, Edited by G. E. Powell, R. H. Bishop, J. B. Lundberg, and R. H. Smith, Univelt, San Diego, California, pp. 839–858, 1996.
12. WAGNER, L. A., JR., and MUNK, M. M., *MISR Interplanetary Trajectory Design*, Spaceflight Mechanics 1996, Edited by G. E. Powell, R. H. Bishop, J. B. Lundberg, and R. H. Smith, Univelt, San Diego, California, pp. 859–876, 1996.
13. LOHAR, F. A., MISRA, A. K., and MATEESCU, D., *Mars–Jupiter Aerogravity Assist Trajectories for High-Energy Missions*, Journal of Spacecraft and Rockets, Vol. 34, No. 1, pp. 16–21, 1997.
14. MIELE, A., *Flight Mechanics, Vol. 1: Theory of Flight Paths*, Addison-Wesley Publishing Company, Reading, Massachusetts, 1962.
15. MIELE, A., HUANG, H. Y., and HEIDEMAN, J. C., *Sequential Gradient-Restoration Algorithm for the Minimization of Constrained Functions: Ordinary and Conjugate Gradient Versions*, Journal of Optimization Theory and Applications, Vol. 4, No. 4, pp. 213–243, 1969.
16. MIELE, A., TIETZE, J. L., and LEVY, A. V., *Comparison of Several Gradient Algorithms for Mathematical Programming Problems*, Omaggio a Carlo Ferrari, Edited by G. Jarre, Libreria Editrice Universitaria Levrotto e Bella, Torino, Italy, pp. 521–536, 1974.
17. MIELE, A., PRITCHARD, R. E., and DAMOULAKIS, J. N., *Sequential Gradient-Restoration Algorithm for Optimal Control Problems*, Journal of Optimization Theory and Applications, Vol. 5, No. 4, pp. 235–282, 1970.
18. MIELE, A., TIETZE, J. L., and LEVY, A. V., *Summary and Comparison of Gradient-Restoration Algorithms for Optimal Control Problems*, Journal of Optimization Theory and Applications, Vol. 10, No. 6, pp. 381–403, 1972.
19. MIELE, A., and DAMOULAKIS, J. N., *Modifications and Extensions of the Sequential Gradient-Restoration Algorithm for Optimal Control Theory*, Journal of the Franklin Institute, Vol. 294, No. 1, pp. 23–42, 1972.
20. HEIDEMAN, J. C., and LEVY, A. V., *Sequential Conjugate Gradient-Restoration Algorithm for Optimal Control Problems, Parts 1 and 2*, Journal of Optimization Theory and Applications, Vol. 15, No. 2, pp. 203–222 and 223–244, 1975.
21. MIELE, A., and WANG, T., *Primal-Dual Properties of Sequential Gradient-Restoration Algorithms for Optimal Control Problems, Part 1: Basic Problem*, Integral Methods in Science and Engineering, Edited by F. R. Payne et al., Hemisphere Publishing Corporation, Washington, DC, pp. 577–607, 1986.
22. MIELE, A., and WANG, T., *Primal–Dual Properties of Sequential Gradient-Restoration Algorithms for Optimal Control Problems, Part 2: General Problem*, Journal of Mathematical Analysis and Applications, Vol. 119, Nos. 1–2, pp. 21–54, 1986.
23. MIELE, A., *Recent Advances in the Optimization and Guidance of Aeroassisted Orbital Transfers*, The 1st John V. Breakwell Memorial Lecture, Acta Astronautica, Vol. 38, No. 10, pp. 747–768, 1996.

24. MIELE, A., and WANG, T., *Near-Optimal Highly Robust Guidance for Aeroassisted Orbital Transfer*, Journal of Guidance, Control, and Dynamics, Vol. 19, No. 3, pp. 549–556, 1996.
25. MIELE, A., and WANG, T., *Robust Predictor–Corrector Guidance for Aeroassisted Orbital Transfer*, Journal of Guidance, Control, and Dynamics, Vol. 19, No. 5, pp. 1134–1141, 1996.
26. RISHIKOF, B. H., MCCORMICK, B. R., PRITCHARD, R. E., and SPONAUGLE, S. J., *SEGRAM: A Practical and Versatile Tool for Spacecraft Trajectory Optimization*, Acta Astronautica, Vol. 26, Nos. 8–10, pp. 599–609, 1992.